

## Monitoring annual urbanization activities in Guangzhou using Landsat images (1987–2015)

Ying Sun, Xinchang Zhang, Yuan Zhao and Qinchuan Xin

School of Geography and Planning, Sun Yat-Sen University, Guangzhou, China

### ABSTRACT

Rapid land-use/land-cover (LULC) changes such as urbanization have tremendous impacts on regional climate and environment. Satellite images acquired by fast-developing remote-sensing techniques provide frequent observations of the land surface, thereby allowing for continuous mapping of urbanization activities. In this study, we investigated the annual urbanization activities over the past three decades in Guangzhou, one of the largest metropolises in China. To enhance the efficiency of training sample extraction in long-term land-cover mapping, we developed a three-step method: 1) three spectral indices were derived to extract the candidates of training samples based on decision trees; 2) a spatial filter was used to extract homogenous samples for each land-cover type; and 3) temporal consistency checking was performed for the samples of urban areas. We applied the developed method to time-series Landsat images and produced annual land-cover maps of Guangzhou from 1987 to 2015. We evaluated the produced land-cover maps and found an average overall accuracy of 89.80% for all studied years. Our results show that dramatic urbanization has occurred in the region of the Guangzhou city, where built-up areas have mostly expanded to the northwest, east, and south of the central regions of Guangzhou. The average growth rate of urban areas in Guangzhou from 1987 to 2015 was at 38.72 km<sup>2</sup> per year, which was generally consistent with the government survey data. Future studies are required to understand how rapid urbanization in Guangzhou influences social economy and environmental sustainability.

### ARTICLE HISTORY

Received 26 March 2016  
Accepted 19 November 2016

## 1. Introduction

Urbanization is often associated with various issues, such as economic development, land-use/land-cover change (LULC), urban land expansion, urban heat islands, and urban population growth (Schneider and Mertens 2014; Georgescu et al. 2014; Gong et al. 2012). Excessive expansion of urban lands could also lead to changes in regional climate and water cycles (Zhou et al. 2004; Shao et al. 2006). Understanding the spatiotemporal pattern of urbanization is important to studies on environmental sustainability and human–environment interactions (Weng 2012; Fan and Deng 2014). In this context,

**CONTACT** Xinchang Zhang  [eeszxc@mail.sysu.edu.cn](mailto:eeszxc@mail.sysu.edu.cn)  School of Geography and Planning, Sun Yat-Sen University, Earth and Environment Building D405, Guangzhou, 510275, China

© 2017 Informa UK Limited, trading as Taylor & Francis Group

mapping regional urbanization not only provides valuable data sets for related scientific studies, but also offers key information to urban planners and government decision-makers (Triantakonstantis et al. 2015; Chrysoulakis et al. 2013a, 2014).

Rapid urbanization has occurred worldwide in recent decades, whereas most of the cities in China have developed dramatically. As the third largest city in China, Guangzhou has experienced rapid growth of urban areas with increased surrounding suburban sprawl. Urbanization in Guangzhou has received a wide range of interests from scientific researchers. Ma and Xu (2010) identified the built-up areas in Guangzhou from 1979 to 2002 and analysed the dominant driving factors underlying the urbanization. Zhang et al. (2010) analysed multi-date digital orthophotographs of Guangzhou and derived mutual conversions among land-use classes using a land-use transfer model. Sun et al. (2013) investigated the urbanization processes of the core area of Guangzhou by combining remote-sensing data and spatial metrics. Fan and Fan (2014) extracted impervious surface areas in Guangzhou from 1990 to 2009 based on linear unmixing analysis. Chen et al. (2016) examined the spatiotemporal changes of urban land areas in Guangzhou from 1980 to 2010 and investigated the spatial factors in determining land conversions. Despite these successful applications, most of the existing studies focused on the central regions of the Guangzhou city, and fine-resolution LULC maps for the entire area of Guangzhou would be valuable for regional studies.

Since the public opening of the Landsat archive at the U.S. Geological Survey (Woodcock et al. 2008), long-term data from Landsat have been widely used for a broad range of applications on land-surface studies (Gutman et al. 2004). The abundant Landsat images offer opportunities to study urban dynamics at finer spatial resolution than moderate- and coarse-resolution satellite data such as Moderate Resolution Imaging Spectroradiometer (MODIS) and Advanced Very High Resolution Radiometer (AVHRR) (Seto et al. 2002; Schneider, Seto, and Webster 2005). Weng (2001) quantified urban growth in the Pearl River Delta based on two individual Landsat Thematic Mapper (TM) images, and then assessed the impacts of urbanization on regional surface temperature. Deng, Fan, and Chen (2012) extracted impervious surface areas of the Pearl River Delta in China using Landsat imagery from 1998 to 2008. Schneider and Mertes (2014) used Landsat images and demographic data to compare the trends of urban expansions and population growth in 142 Chinese cities at a coarse time interval from 1978 to 2010. Chen et al. (2015) used Landsat data to generate a 30 m global land-cover product, which included maps of urban areas in China. Owing to large data volume and long processing time, studies that cover a long spanning period tend to map the land covers at relatively coarse time intervals (e.g. 5 years or more), whereas continuous mapping of time-series LULC in urban areas is often needed by various end users.

To map urban dynamics, various methods have been developed, including pixel-based classification (Bauer et al. 2004), subpixel classification (Li et al. 2013; Mitraka et al. 2012), object-oriented approaches (Vieira et al. 2012), and machine-learning algorithms (Foody, McCulloch, and Yates 1995; Hu and Weng 2009; Chrysoulakis et al. 2013b). Poursanidis, Chrysoulakis, and Mitraka (2015) applied both pixel-based and object-based methods to Landsat images for urban land-cover classification and found that the pixel-based method could perform better than the object-based method. Gao et al. (2012) manually identified the training samples for each image, and then used stacked Landsat maps to expand the training samples based on spectral distances by assuming

that urban land conversion is irreversible. Li, Gong, and Liang (2015) collected training data through visual interpretation based on high-resolution imagery from Google Earth. Deng and Wu (2013) developed automated algorithms to obtain relatively pure endmembers for subpixel classification. Somers et al. (2012) grouped randomly selected pure endmembers by a clustering technique as inputs to subpixel classification. Overall, in the long-term LULC mapping studies, training sample extraction is often labour-intensive, making it time-consuming to produce and evaluate the classification maps.

The objectives of this study are to: (1) develop a method to enhance the efficiency of training sample extraction for pixel-based classification, and (2) map the urban dynamics of the entire Guangzhou city at a relatively high temporal resolution from 1987 to 2015 using Landsat images.

## 2. Study area and data preprocessing

Guangzhou, the capital of the Guangdong province, is located alongside the Pearl River in South China. Largely due to increased investments in the coastal open cities, Guangzhou now ranks the third largest city in China. The city of Guangzhou consists of 11 administrative districts and occupies an area of 7434 km<sup>2</sup> (Figure 1). Although many studies (Fan and Fan 2014; Chen et al. 2016) have paid attention to the increased core urban areas in Guangzhou municipality, rapid urban expansion has also occurred at the city fringe. The entire Guangzhou municipality represents an ideal case of the fast-developing urban areas for study.

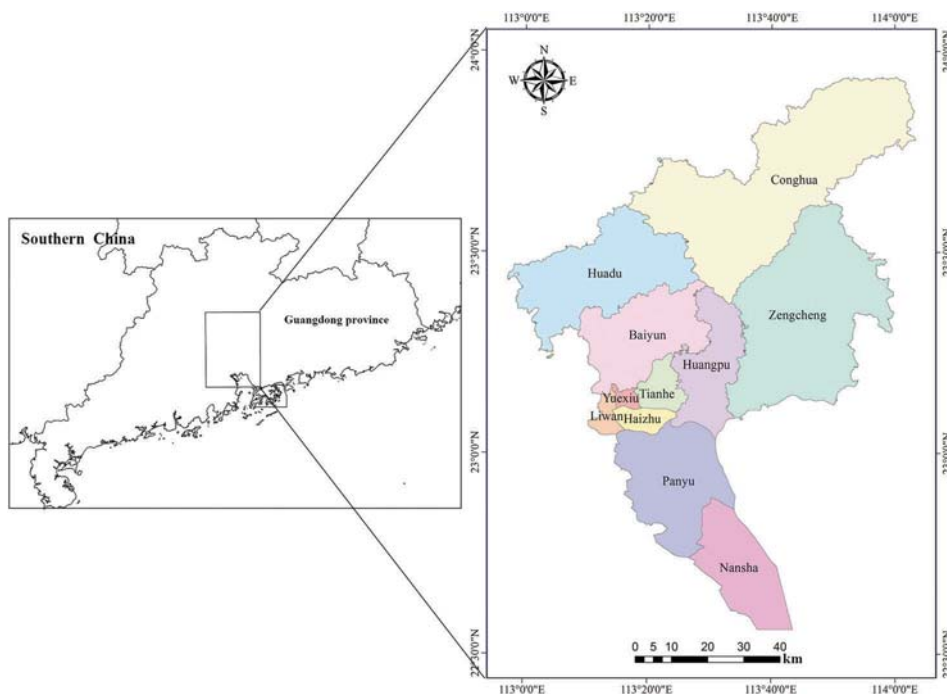


**Figure 1.** The study area of Guangzhou city in southern China.

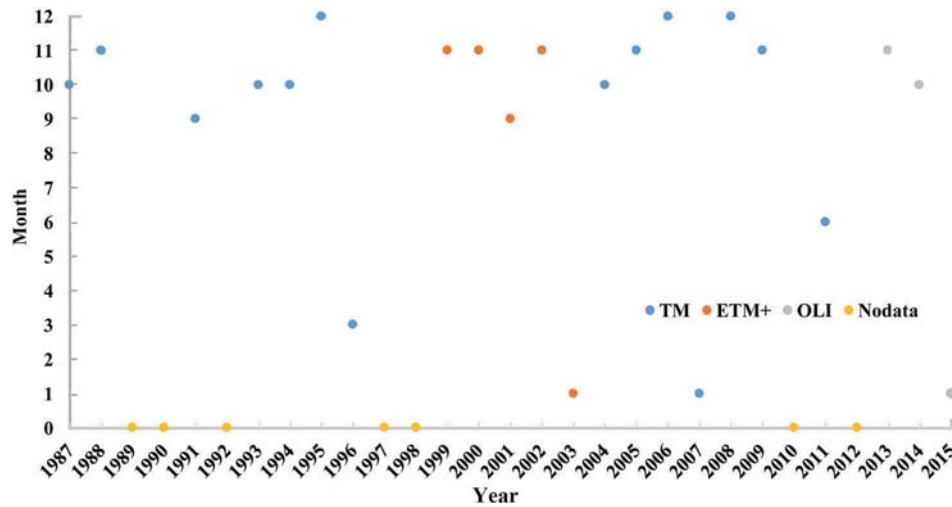


**Figure 2.** The temporal distribution of the used Landsat TM/ETM+/OLI images.

Two Landsat scenes (Path/Row: 122/44 and 122/43) are needed to cover the entire study area. Because of persistent cloud cover in the subtropical area, the available Landsat images are much fewer in Guangzhou than in other places in the temperate areas in China. We used images with slight cloud cover (the highest cloud cover is about 5%, whereas most of the clouds presented at the Pearl River estuary with few effects on mapping the built-up areas) for analysis and obtained 43 images of Landsat 4–5 TM, Landsat Enhanced Thematic Mapper Plus (ETM+), and Landsat Operational Land Imager (OLI) (Figure 2) that covered the period spanning from 1987 to 2015. All Landsat images at Level 1 T were downloaded from the U.S. Geological Survey Earth Explorer (<http://glovis.usgs.gov/>) and GSCloud (<http://www.gscloud.cn/>). There remain seven years (1989, 1990, 1992, 1997, 1998, 2010, and 2012) and one scene (122/43) in 1988 with no available cloud-free images during our study period. Because Guangzhou has a subtropical climate and many plant species are evergreen, most of the cloud-free images were acquired in autumn and winter. In sum, we used 18 images in autumn and 17 images in winter, and only two images in spring and six images in summer.

We performed atmospheric correction with the Fast Line-of-sight Atmospheric Analysis of Spectral Hypercubes (FLAASH, Anderson et al. 2002). We used the season-latitude information to select the appropriate Moderate Resolution Atmospheric Transmission (MODTRAN) model (Berk et al. 1998). Based on visual examination, all images have the correct geometric coordinates, except the images acquired in 1995. Therefore, the images acquired in 1995 were registered to the images acquired in 2000, and the resulting root mean square error of image rectification was less than 0.5 pixels. Individual scenes were mosaicked based on the nearest-neighbour resampling method. The mosaicked images were further subset by the administrative boundaries of the Guangzhou city for subsequent analysis.

### 3. Methods

Figure 3 illustrates the framework of our study, and the main steps are to: (1) develop decision trees based on spectral indices derived from Landsat data; (2) extract training sample candidates automatically based on the developed methods; (3) perform temporal consistency checking for the extracted urban land training samples and filter all training samples; and (4) derive and analyse the land-cover maps of Guangzhou on an annual basis from 1987 to 2015 using a supervised classifier.

#### 3.1. Definition of land-cover types

Because our primary interests are to map urban dynamics, we identified four types of land covers, including vegetation, bare soil, urban land, and waterbody. The class of vegetation mainly includes areas that are covered with tall trees, shrubs, grass, farmland, and orchard; the class of bare soil includes exposed soil surfaces with little vegetation cover, such as deforested lands, abandoned farmlands, quarries, and naturally unvegetated areas; the class of urban land is defined as built environment with impervious surfaces (Li, Gong, and Liang 2015; Schneider and Mertes 2014) dominated by man-made structures such as buildings and transportation facilities; and the class of waterbody includes areas of open water such as rivers and ponds.

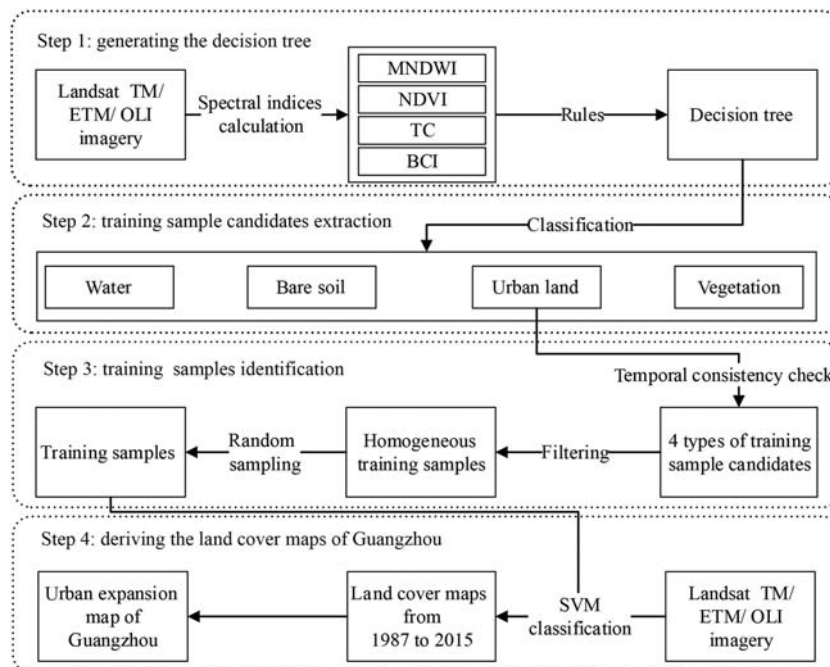


Figure 3. The overall framework of the study.

### 3.2. Automatic extraction of training sample candidates

Training sample selection is a challenging task in long-term and high-frequency LULC mapping. In this study, a method was proposed to enhance the efficiency of training sample extraction. Three spectral indices, modified normalized difference water index (MNDWI, Xu 2005), normalized difference vegetation index (NDVI, Rouse et al. 1973), and biophysical composition index (BCI, Deng and Wu 2012), were adopted to separate the four types of land cover.

MNDWI has proved effective to enhance the differences of spectral signals between waterbodies and the built-up areas or vegetated lands. Typically, waterbody has high values of MNDWI, whereas vegetation and other types of land cover have low values. MNDWI is derived based on reflectance values ( $R$ ) for the green and shortwave infrared bands:

$$\text{MNDWI} = \frac{(R_{\text{Green}} - R_{\text{MIR1}})}{(R_{\text{Green}} + R_{\text{MIR1}})} \quad (1)$$

NDVI has shown to be positively correlated to vegetation chlorophyll content and thus has been widely used to distinguish vegetation cover from non-vegetated areas. NDVI is derived based on reflectance values ( $R$ ) for red and near infrared bands:

$$\text{NDVI} = \frac{(R_{\text{NIR}} - R_{\text{Red}})}{(R_{\text{NIR}} + R_{\text{Red}})} \quad (2)$$

It is difficult to separate the classes between bare soil and urban land using the spectral bands of remote-sensing images (Zhang, Chen, and Lu 2015). Among efforts that have been made to derive specific spectral indices for identifying urban lands from bare soil (Rikimaru 1996; Zha, Gao, and Ni 2003; Xu 2010), BCI shows to be indicative to impervious surface (Deng and Wu 2012). Based on the Tasseled Cap (TC) transformation, which compresses the multispectral data into a few bands that are associated with physical scene characteristics (Crist and Cicone 1984), BCI is derived in a similar way to Ridd's conceptual vegetation-impervious surface-soil (V-I-S) model (Ridd 1995) by normalizing the TC spectra as follows:

$$\begin{aligned} \text{BCI} &= \frac{(H+L)/2-V}{(H+L)/2+V}, \\ \text{with} \\ H &= \frac{(\text{TC})_1 - (\text{TC})_{1,\min}}{(\text{TC})_{1,\max} - (\text{TC})_{1,\min}}, \\ V &= \frac{(\text{TC})_2 - (\text{TC})_{2,\min}}{(\text{TC})_{2,\max} - (\text{TC})_{2,\min}}, \\ L &= \frac{(\text{TC})_3 - (\text{TC})_{3,\min}}{(\text{TC})_{3,\max} - (\text{TC})_{3,\min}}, \end{aligned} \quad (3)$$

where  $(\text{TC})_i$  ( $i = 1, 2,$  and  $3$ ) denote the first three components of the TC transformation, and the subscripts of min and max denote the minimum and maximum values of each TC component in the corresponding image. Because the band coefficients for the TC transformation could vary with sensors, we applied different TC models for the Landsat TM (Crist and Cicone 1984), ETM+ (Huang et al. 2002), and OLI data (Baig et al. 2014) in our study.

A decision tree classifier was then developed based on the input spectral indices (Figure 4). The thresholds to separate classes of land covers for each individual image were determined by Otsu's thresholding method (Otsu 1979), which automatically

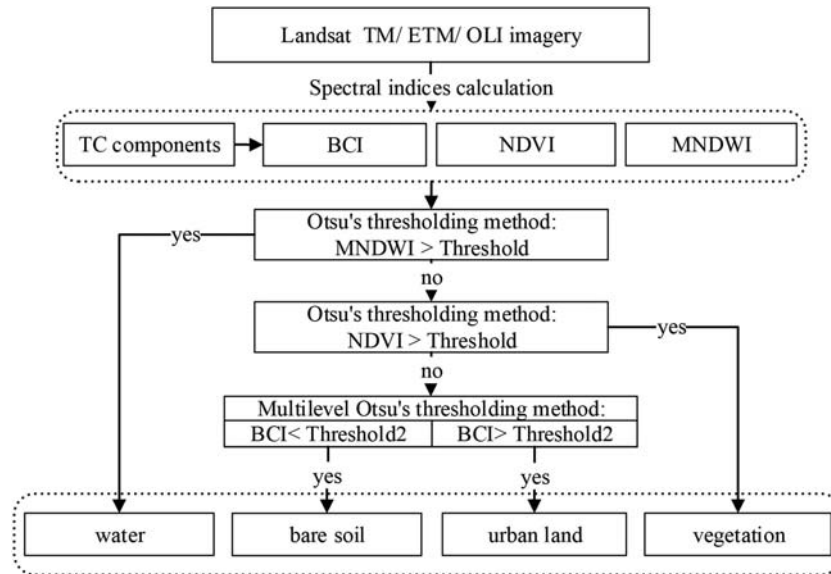


**Figure 4.** A work flow showing the decision tree used for automated extraction of training sample candidates.

searches the optimal thresholding values that minimize the intra-class variance between two individual classes. Waterbodies and vegetation were first identified based on MNDWI and NDVI, and then the multilevel Otsu's thresholding method (Huang and Wang 2009) was applied for the separation of urban land, bare soil, and background (a small proportion of pixels consists of mixed land-cover types). In this way, each Landsat image was preliminarily classified into four land-cover types for obtaining the training sample candidates.

The quality of training samples largely affects the results of the supervised classification (Gao et al. 2012). We considered a pixel to have high probability to be a pure endmember if surrounded by neighbours with the same land-cover type. To ensure the spatial homogeneity, a window size of  $5 \times 5$  pixels (Deng and Wu 2013) was applied to filter the training sample candidates and obtain relatively homogeneous sample candidates. After the processing, we found that there was little confusion among classified land-cover types except for urban land. Therefore, 300 training samples were extracted for each land-cover type from the filtered candidates of training samples by a random sampling method, whereas urban training samples are further processed with temporal consistency checking as described in details in the next section.

### 3.3. Temporal consistency check for training samples of urban lands

Among the defined land-cover types, bare soil is often misidentified as urban land, especially in rural areas. Note that urban land typically will not be converted to other land-cover types in a short time period. Gao et al. (2012) considered that the process of urban land expansion was irreversible. Li, Gong, and Liang (2015) checked the time series data to identify misclassified urban lands and improve the overall land-cover

classification. Here, we implemented a process of temporal consistency checking to identify accurate training samples of urban land.

Many of the misclassifications between bare soil and urban land are due to crop rotations in croplands. Therefore, if a pixel is misclassified as urban land in an earlier year but identified as vegetation in a later year, the corresponding pixel is considered as bare soil in the earlier year and vegetation in the later year. When performing the temporal consistency checking, the images acquired in 1987 and 2015 were first classified to provide general masks of non-urban areas. A removal scheme was applied to eliminate incorrect urban training sample candidates in the years from 1988 to 2014 based on the irreversibility of urban land. By using the 1987 and 2015 non-urban land masks, urban training sample candidates in 1988 were first obtained and further filtered by a window size of  $5 \times 5$  pixels to ensure the spatial homogeneity. As urban areas increase year by year, it is best to extract samples of both already-existing and newly developed urban land for accurate classification. Accordingly, screened candidates in 1988 were masked by non-urban land areas in 1987 to separate the urban land in 1987 from the urban land newly developed between 1987 and 1988. Eventually, 300 urban land samples were randomly selected for each year, among which 80% were from the original urban land candidates and 20% from the new ones. In a similar manner, the processes were incrementally applied to the other years in between 1987 and 2015 to obtain the urban land candidates for each individual image.

### **3.4. Classification**

Based on the Landsat data and the training samples, we applied a pixel-based supervised classifier, the Support Vector Machine (SVM, Vapnik 1995, 1998), to classify the land-cover types for each individual pixel. SVM is essentially a machine-learning algorithm to solve nonlinear classification problems with small data sets based on the principle of structural risk minimization and has proved useful in the field of remote sensing. The basic idea of the algorithm is to develop optimal hyperplanes that separate the classes by mathematically transforming nonlinear input data into the high-dimensional feature space (Boser, Guyon, and Vapnik 1992). Kernel functions are introduced in SVM to reduce the computational loading in higher dimensional space (Vapnik 1995). SVM has been recognized as an effective classifier in land-cover mapping and some details on SVM could be found in Huang, Davis, and Townshend (2002) and Chang and Lin (2011). We used the ENVI (the environment for visualizing images software) SVM classifier in this study and the parameter settings were as follows: the radial basis function was used as the kernel type, the gamma in the kernel function was set as 0.143, and the penalty parameter was set as 100.

## **4. Results and discussion**

### **4.1. Spectral indices analysis and training sample extraction**

Figure 5 shows examples for a subset of the image in 2007 (Figure 5(a)) and the extracted corresponding spectral indices. For MNDWI (Figure 5(b)), waterbodies have the highest values, vegetation has the lowest values, and the other land-cover types have moderate

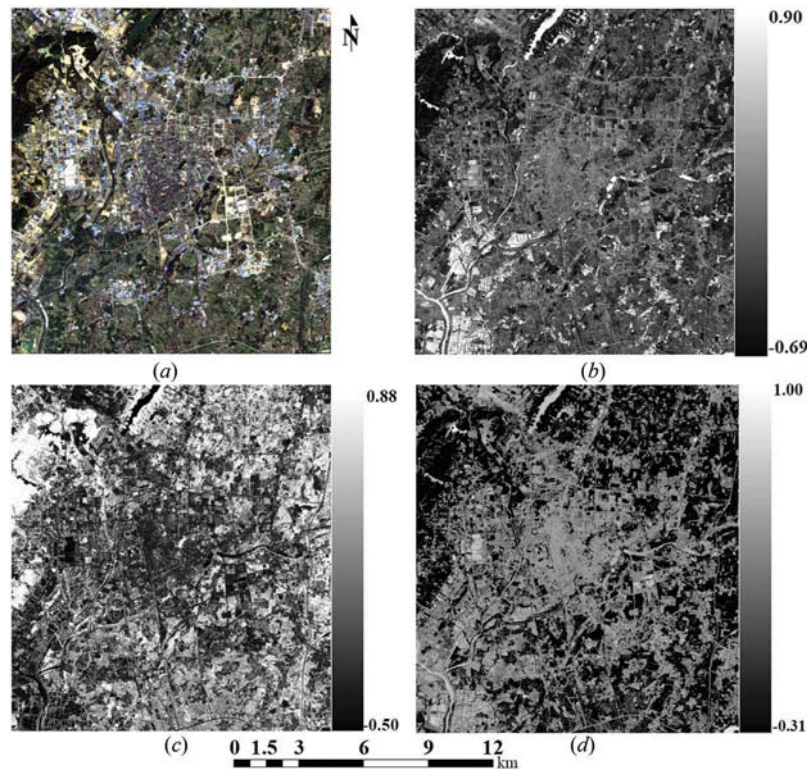


**Figure 5.** Examples are shown for (a) the true-colour composite, (b) MNDWI, (c) NDVI, and (d) BCI of a subset of the Landsat image acquired in 2007.

values. NDVI shown in Figure 5(c) well identified the vegetation cover. The BCI image shown in Figure 5(d) could separate urban lands and bare soil. Specifically, pixels with high values of BCI (light grey and moderate grey) are urban land and waterbodies, pixels with inter-medium values of BCI (dark grey and black) are associated with bare soil, and pixels with low values of BCI (black colour) are mostly vegetated areas.

The different features in the spectral indices provide a basis to extract training sample candidates for each land-cover type except the class of urban land. To demonstrate the extraction of urban land candidates, Figure 6 shows an example for the year of 2007. Urban land candidates (maroon pixels) of 2007 were initially extracted based on the analysis of spectral indices (Figure 6(a)). Most soil backgrounds were successfully separated from urban land areas, but apparent misclassification still exists, especially in the rural areas, largely due to the within-class and between-class variation of spectral signals. Candidates of urban training sample candidates in Figure 6(a) were screened by the non-urban land mask in 2015. As a result, incorrect candidates were largely removed (see Figure 6(b)). To ensure the spatial homogeneity and increase the confidence of representative endmembers, candidates of urban land pixels in Figure 6(b) were further filtered by a window size of  $5 \times 5$  pixels. Homogeneous patches were retained and spatially scattered points were cleaned, whereas the remaining pixels in the results are shown in Figure 6(c) (note that some remaining pixels are too small to be seen clearly). The mask for the filtered urban land in 2006 was applied to determine the

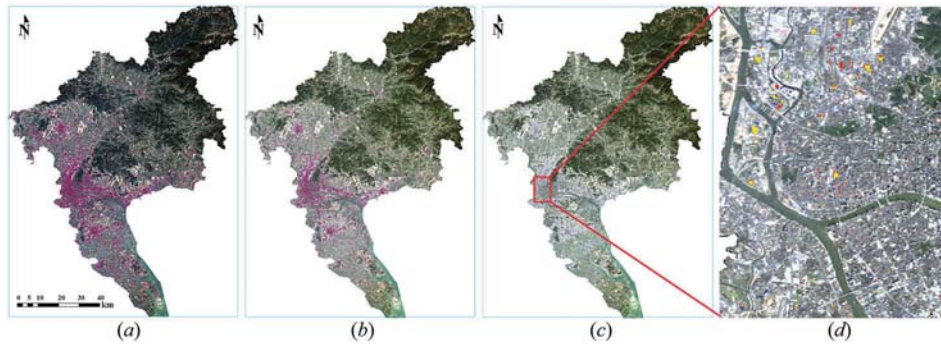


**Figure 6.** Examples to illustrate the extraction of urban training samples are shown for (a) the initial training sample candidates of urban land, (b) training sample candidates of urban land after performing the temporal consistency checking, (c) training sample candidates of urban land after filtering with the  $5 \times 5$  pixel window, and (d) a close view of the training samples for both already-existing and newly developed urban land. In Figure 6d, the blue pixels are training samples for 2006, the red ones are training samples for 2007, and the yellow ones are training samples for both 2006 and 2007.

**Table 1.** The Jeffries–Matusita distances of the samples for different land-cover types as obtained for the years of 2006 and 2007.

Year	Land-cover type	Bare soil	Urban land	Water	Vegetation
2006	Bare soil	–	1.880	1.991	1.971
	Urban land	1.880	–	1.999	1.989
	Water	1.991	1.999	–	1.987
	Vegetation	1.971	1.989	1.987	–
2007	Bare soil	–	1.929	1.999	1.982
	Urban land	1.929	–	1.999	1.993
	Water	1.999	1.999	–	1.999
	Vegetation	1.982	1.993	1.999	–

candidates of already-existing and newly developed urban land (Figure 6(d)). The yellow pixels represent urban training samples for both 2006 and 2007, and the blue and red pixels are urban training samples for 2006 and for 2007, respectively. In total, 300 training samples were extracted by the random sampling method from the pixels shown in yellow and red colours in Figure 6(d). To understand the representative of the land-cover training samples, Table 1 shows the derived values of the Jeffries–Matusita distance (Swain and Davis 1978), a metric that is indicative of the separability among classes, for the samples of different land-cover types in the years of 2006 and 2007. The Jeffries–Matusita distances are all greater than 1.85, indicating that the training samples of different land-cover classes vary largely in terms of the spectral signals. Because bare soil and urban land could be misclassified in an individual image, temporal consistency checking helps improve the selection of the training samples, thereby reducing potential misclassification errors.

#### 4.2. Classification and evaluation

The land-cover types were classified with the automatically extracted training samples using the SVM classifier (Figure 7). Based on visual inspection, the classification results

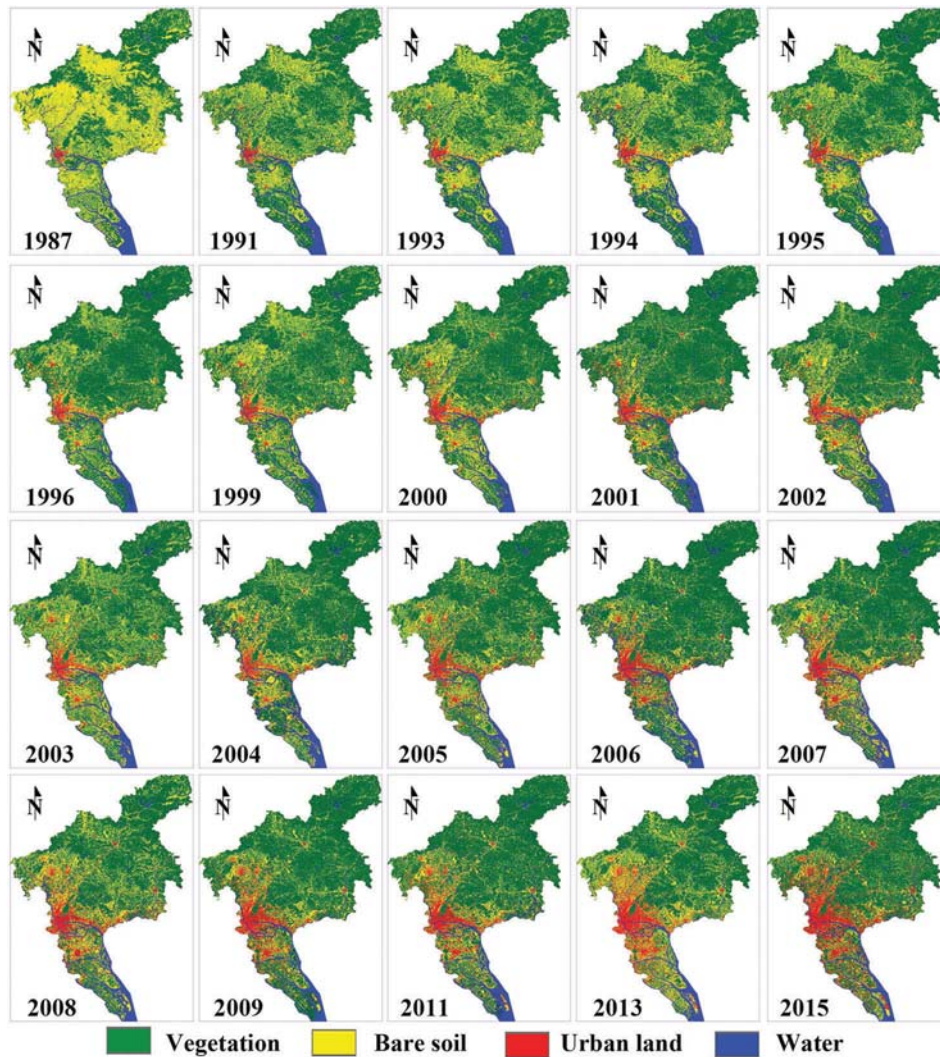


**Figure 7.** Land-cover distribution maps of Guangzhou from 1987 to 2015 on an annual basis as derived from Landsat time series images.

well capture the spatial pattern of land-cover distributions in each year. Vegetation coverage in the northern mountainous areas was relatively low before the 1990s. Benefiting from the reforestation project in southern China, green hills and grass-covered areas increased in the later years of the study period. At the same time, urbanization in Guangzhou is evident as urban land largely expanded to the north, east, and south of the city centre. The urban land in Guangzhou almost continuously increased from year to year, and the derived areas of urban land for the entire Guangzhou city in 2015 were nearly as many as six times of that in 1987.

Taking the years of 1987, 1995, 2005, and 2014 as examples, Table 2 shows the confusion matrices that are indicative of the accuracy of the land-cover classification results. To support the accuracy assessment, 120 samples for each land-cover type were

**Table 2.** The confusion matrices of the land-cover classification results are shown for the years of 1988, 1995, 2005, and 2014.

Year	Land-cover type	Reference data				PA (%)	UA (%)
		Bare soil	Urban land	Water	Vegetation		
1988	Bare soil	116	24	2	3	96.67	80.00
	Urban land	0	86	0	0	71.67	100.00
	Water	2	4	103	0	85.83	94.50
	Vegetation	2	6	15	117	97.50	83.57
	Overall accuracy = 87.92%; $\kappa = 0.84$						
1995	Bare soil	100	19	0	1	83.33	83.33
	Urban land	0	97	1	1	80.83	97.98
	Water	1	0	115	1	95.83	98.29
	Vegetation	19	4	4	117	97.50	81.25
	Overall accuracy = 89.38%; $\kappa = 0.86$						
2005	Bare soil	110	15	8	4	91.67	80.29
	Urban land	4	102	3	4	85.00	90.27
	Water	0	2	104	0	86.67	98.11
	Vegetation	6	1	5	112	93.33	90.32
	Overall accuracy = 89.17%; $\kappa = 0.86$						
2014	Bare soil	108	10	2	2	90.00	88.52
	Urban land	6	102	6	1	85.00	88.70
	Water	2	2	110	1	91.67	95.65
	Vegetation	4	6	2	116	96.67	90.63
	Overall accuracy = 90.83%; $\kappa = 0.88$						

PA and UA denote the producer's accuracy and the user's accuracy, respectively.

randomly selected and visually interpreted based on Landsat images and high-resolution Google Earth images. As summarized in Table 2, misclassification mainly occurred between the classes of bare soil and urban land, and between the classes of vegetation and bare soil. In the year of 1988, some pixels of urban land were misidentified as bare soil because of the similar spectral signatures of bright urban land and dry bare soil. In the years of 2005 and 2014, the spectral signature of soil background was found to be similar to that of dark urban land, possibly due to high soil moisture. Misclassification between the classes of bare soil and vegetation was mainly due to low vegetation coverage over the dry soil background. Mountain shadows in the northern mountain area could be occasionally misclassified as waterbodies, but would not influence our study on urban expansion. The values of the producer's and user's accuracies (Story and Congalton 1986) vary from class to class and from year to year, whereas both overall accuracies and kappa coefficient ( $\kappa$ ) (Rosenfield and Fitzpatrick-Lins 1986) are consistently high for different years. Figure 8 provides the time series of the overall accuracies for the land-cover classification. On average, the overall accuracy is approximately 89.80% and maintains consistently high above roughly 85.0%, demonstrating that the land-cover classification results provide a solid basis for quantifying urbanization activities in the fast-developing urban areas.

The variation of the total urban land areas as derived from the Landsat images is shown in Figure 9. The orange line represents the derived urban land areas for the entire Guangzhou city. Missing data in the time series, for example, 2010 and 2012, are resulted by unavailable Landsat images due to persistent cloud cover. Two types of official statistics obtained based on ground survey were used for comparisons. The short blue line denotes the official urban area data for the most recent five years (2010–2014) excluding Conghua and Zengcheng (two districts located in the administrative division

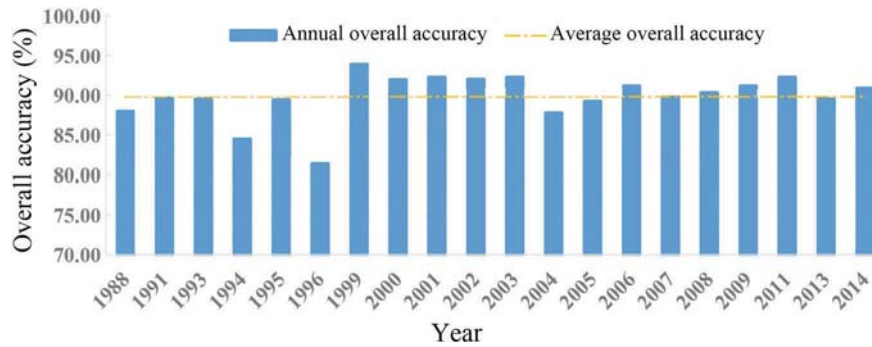


**Figure 8.** The overall accuracies of the classification maps for different years.

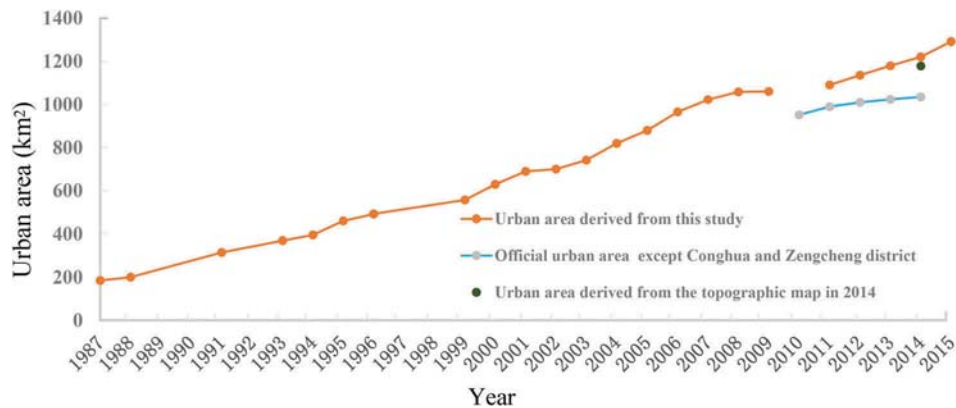


**Figure 9.** Comparison of the total areas of urban land as derived from Landsat images, reported by the Guangzhou City Planning and Automation Center (without the districts of Conghua and Zengcheng), and derived from the topographic map produced by the Guangzhou Urban Planning and Design Survey Research Institute.

of Guangzhou) as reported by the Guangzhou City Planning Automation Center (no data were released before 2010). Comparison of both orange and blue lines implies that areas of urban land derived from Landsat images agree with those obtained from the survey data in general. The urban land areas derived by Landsat-based analysis are higher than the values released by official reports, because the districts of Conghua and Zengcheng were not included in the official reports and because the pixel mixture effects of the Landsat images could lead to biased estimates of urban land areas. In addition to the above-mentioned efforts, we derived the total urban area (shown as the single green point in Figure 9) from a topographic map of 2014 produced by the Guangzhou Urban Planning and Design Survey Research Institute. The urban areas derived from the topographic map agreed well with our mapping results, and the differences of urban areas are as small as 35.72 km<sup>2</sup> (percentage errors are less than 3%). Comparison between the urban areas derived from Landsat with those from other ancillary data indicates that the long-term dynamics of urban development in Guangzhou is well captured.

Urban areas in Guangzhou have increased rapidly during the past 30 years. The derived urban areas were approximately 200 km<sup>2</sup> in 1987, but grew to above 1200 km<sup>2</sup> in 2015. When fitting with a simple linear trend, the annual growth rate of the urban areas derived from Landsat images was approximately 38.72 km<sup>2</sup> per year from 1987 to 2015. Although the urban areas appeared to increase continuously during the past 30 years in Guangzhou, the increasing rates could vary in specific periods. For example, there were slight slowdown periods such as 2001–2004, and fast-growing periods such as 2005–2010. To understand the spatial pattern of the urban development, we show the map of urban expansion from 1987 to 2015 in Figure 10 at aggregated time intervals of approximately 5 years (depending on the availability of the Landsat images). Built-up areas in 1987 were mainly located in the Midwest of Guangzhou and spread in the urban fringe surrounding the city centre. Over the past three decades, the urban area of Guangzhou gradually expanded to the peripheral regions, and lots of newly developed urban land occurred in the northwest, east, and south parts of Guangzhou. Guangzhou appears to develop from single-core to multicore spatial distributions of the urban cities. The uneven growing rates of urban areas in the

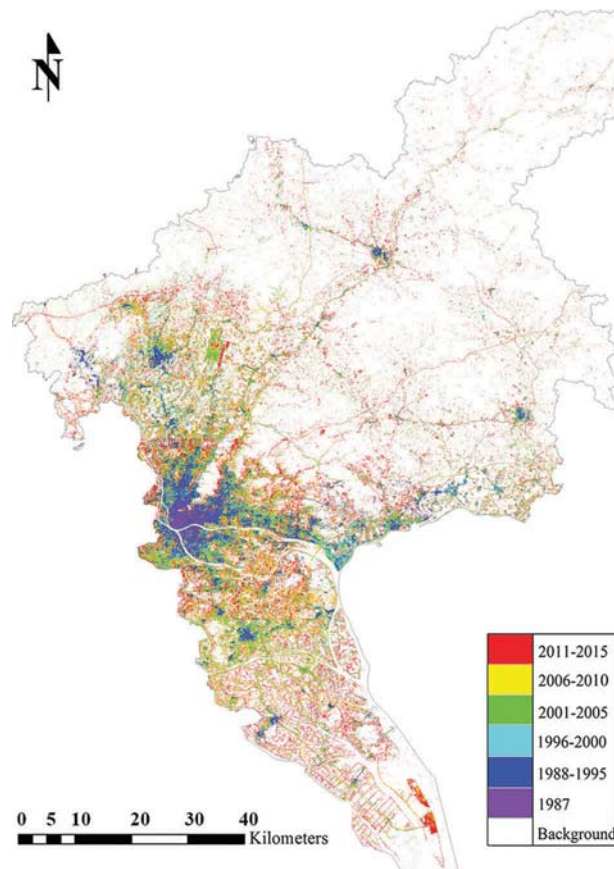


**Figure 10.** The map of urban expansion in Guangzhou from 1987 to 2015 as derived from the Landsat data.

study period were likely related to the immigration of rural population into Guangzhou in previous studies (Zhang et al. 2010). Obviously, a number of social economy and policy factors could play a role in the process of urban expansion, for example, the policy to integrate counties (such as Panyu, Huadu, Nansha, Conghua, and Zengcheng) into administrative districts of Guangzhou could stimulate rapid expansion. How urban expansion interacts with social economy and exerts impacts on environmental sustainability is beyond the scope of the current study, but is of interest to investigate with synthesized modelling in the future research.

## 5. Conclusion

To understand the dynamics of fast-developing urban areas at finer spatial and temporal resolution, we investigate the Guangzhou city in south China using time series of Landsat data from 1987 to 2015. Because long-term and high-frequency mapping of LULC involves labour-intensive processes of sample selection, we developed a three-step method that allows for the automated extraction of training samples for each individual Landsat image. 1) A decision tree based on three spectral indices (i.e. MNDWI, NDVI, and BCI) is built to initially classify the land-cover types and obtain training sample candidates. 2) A spatial filter of the pixel window is applied to screen out relatively heterogeneous sample candidates. 3) Temporal consistency checking is further performed to screen the sample candidates in order to reduce inconsistent training samples of urban land.

We applied our method to the time series of Landsat images and produced classification maps for Guangzhou on an annual basis from 1987 to 2015. The maps of land-cover classification were evaluated against randomly selected sample points. The overall accuracy is consistently high from year to year and has an average value of 89.80% for all study years. Analysis of the results shows that the urban areas derived from Landsat images generally match the reported urban areas during the period of 2010–2014, and agree well with the urban areas derived from the topographic map in 2014. The developed method could potentially be applied to other multispectral images such as MODIS, but it requires further tests because how the differences in the spatial resolution of sensors would influence the land-cover classification results is still largely unclear to date. Based on the land-cover maps produced from Landsat data, urban areas in Guangzhou increased from approximately 200 km<sup>2</sup> in 1987 to over 1200 km<sup>2</sup> in 2015 (more than 600% in equivalence), reflecting the tremendous and rapid processes of regional urbanization. Future studies are needed to understand the underlying drivers behind the urbanization process and subsequent consequences on social economy and environmental sustainability.

## Acknowledgements

We thank the anonymous reviewers for their constructive comments. This research was supported by National Natural Science Foundation of China (grant nos. 41431178, 41401484, and 41671453) and Natural Science Foundation of Guangdong province, China (grant no. 2016A030311016).

## Disclosure statement

No potential conflict of interest was reported by the authors.

## Funding

This work was supported by the National Natural Science Foundation of China [Grant Numbers: 41401484, 41431178, and 41671453]; Natural Science Foundation of Guangdong province, China [Grant Number: 2016A030311016].

## Reference

- Anderson, G. P., G. W. Felde, M. L. Hoke, A. J. Ratkowski, T. W. Cooley, J. H. Chetwynd Jr., J. A. Gardner, et al. 2002. "MODTRAN4-Based Atmospheric Correction Algorithm: FLAASH (Fast Line-Of-Sight Atmospheric Analysis of Spectral Hypercubes)." *Algorithms and Technologies for Multispectral, Hyperspectral, and Ultraspectral Imagery VIII* 4725: 65–71. doi:10.1117/12.478737.
- Baig, M. H. A., L. Zhang, T. Shuai, and Q. Tong. 2014. "Derivation of a Tasseled Cap Transformation Based on Landsat 8 At-Satellite Reflectance." *Remote Sensing Letters* 5 (5): 423–431. doi:10.1080/2150704X.2014.915434.
- Bauer, M. E., N. J. Heinert, J. K. Doyle, and F. Yuan. 2004. "Impervious Surface Mapping and Change Monitoring Using Landsat Remote Sensing." ASPRS annual conference proceedings, Denver, CO, May.
- Berk, A., L. S. Bernstein, G. P. Anderson, P. K. Acharya, D. C. Robertson, J. H. Chetwynd, and S. M. Adler-Golden. 1998. "MODTRAN Cloud and Multiple Scattering Upgrades with Application to AVIRIS." *Remote Sensing of Environment* 65: 367–375. doi:10.1016/S0034-4257(98)00045-5.
- Boser, B. E., I. M. Guyon, and V. N. Vapnik. 1992. "Training Algorithm for Optimal Margin Classifiers." Proceedings of the 5th Annual ACM Workshop on Computational Learning Theory, New York, July 144–152.
- Chang, C. C., and C. J. Lin. 2011. "LIBSVM: A Library for Support Vector Machines." *ACM Transactions on Intelligent Systems and Technology (TIST)* 2 (3): 27. doi:10.1145/1961189.1961199.
- Chen, J., J. Chen, A. Liao, X. Cao, L. Chen, X. Chen, C. He, et al. 2015. "Global Land Cover Mapping at 30m Resolution: A POK-Based Operational Approach." *ISPRS Journal of Photogrammetry and Remote Sensing* 103: 7–27. doi:10.1016/j.isprsjrs.2014.09.002.
- Chen, Y., K. T. Chang, F. Han, D. Karacsonyi, and Q. Qian. 2016. "Investigating Urbanization and Its Spatial Determinants in the Central Districts of Guangzhou, China." *Habitat International* 51: 59–69. doi:10.1016/j.habitatint.2015.10.013.
- Chrysoulakis, N., C. Feigenwinter, D. Triantakoustantis, I. Penyeveskiy, A. Tal, E. Parlow, G. Fleishman, S. Düzgün, T. Esch, and M. Marconcini. 2014. "A Conceptual List of Indicators for Urban Planning and Management Based on Earth Observation." *ISPRS International Journal of Geo-Information* 3 (3): 980–1002. doi:10.3390/ijgi3030980.
- Chrysoulakis, N., M. Lopes, R. San José, C. S. B. Grimmond, M. B. Jones, V. Magliulof, and J. E. M. Klostermann. 2013a. "Sustainable Urban Metabolism as a Link between Bio-Physical Sciences and Urban Planning: The BRIDGE Project." *Landscape and Urban Planning* 112: 100–117. doi:10.1016/j.landurbplan.2012.12.005.
- Chrysoulakis, N., Z. Mitraka, M. Stathopoulou, and C. Cartalis. 2013b. "A Comparative Analysis of the Urban Web of the Greater Athens Agglomeration for the Last 20 Years Period on the Basis of Landsat Imagery." *Fresenius Environmental Bulletin* 22: 2139–2144.
- Crist, E. P., and R. C. Cicone. 1984. "A Physically-Based Transformation of Thematic Mapper Data—The TM Tasseled Cap." *IEEE Transactions On Geoscience and Remote Sensing*, 3: 256–263. doi:10.1109/TGRS.1984.350619.
- Deng, C., and C. Wu. 2012. "BCI: A Biophysical Composition Index for Remote Sensing of Urban Environment." *Remote Sensing of Environment* 127: 247–259. doi:10.1016/j.rse.2012.09.009.

- Deng, C., and C. Wu. 2013. "A Spatially Adaptive Spectral Mixture Analysis for Mapping Subpixel Urban Impervious Surface Distribution." *Remote Sensing of Environment* 133: 62–70. doi:10.1016/j.rse.2013.02.005.
- Deng, Y., F. Fan, and R. Chen. 2012. "Extraction and Analysis of Impervious Surfaces Based on a Spectral Un-Mixing Method Using Pearl River Delta of China Landsat TM/ETM+ Imagery from 1998 to 2008." *Sensors* 12 (2): 1846–1862. doi:10.3390/s120201846.
- Fan, F., and Y. Deng. 2014. "Enhancing Endmember Selection in Multiple Endmember Spectral Mixture Analysis (MESMA) for Urban Impervious Surface Area Mapping Using Spectral Angle and Spectral Distance Parameters." *International Journal of Applied Earth Observation and Geoinformation* 33: 290–301. doi:10.1016/j.jag.2014.06.011.
- Fan, F., and W. Fan. 2014. "Understanding Spatial-Temporal Urban Expansion Pattern (1990–2009) Using Impervious Surface Data and Landscape Indexes: A Case Study in Guangzhou (China)." *Journal of Applied Remote Sensing* 8 (1): 083609–083609. doi:10.1117/1.JRS.8.083609.
- Foody, G. M., M. B. McCulloch, and W. B. Yates. 1995. "Classification of Remotely Sensed Data by an Artificial Neural Network: Issues Related to Training Data Characteristics." *Photogrammetric Engineering and Remote Sensing* 61 (4): 391–401.
- Gao, F., E. B. De Colstoun, R. Ma, Q. Weng, J. G. Masek, J. Chen, Y. Pan, and C. Song. 2012. "Mapping Impervious Surface Expansion Using Medium-Resolution Satellite Image Time Series: A Case Study in the Yangtze River Delta, China." *International Journal of Remote Sensing* 33 (24): 7609–7628. doi:10.1080/01431161.2012.700424.
- Georgescu, M., P. E. Morefield, B. G. Bierwagen, and C. P. Weaver. 2014. "Urban Adaptation Can Roll Back Warming of Emerging Megapolitan Regions." *Proceedings of the National Academy of Sciences* 111 (8): 2909–2914. doi:10.1073/pnas.1322280111.
- Gong, P., S. Liang, E. J. Carlton, Q. Jiang, J. Wu, L. Wang, and J. V. Remais. 2012. "Urbanisation and Health in China." *The Lancet* 379 (9818): 843–852. doi:10.1016/S0140-6736(11)61878-3.
- Gutman, G., A. C. Janetos, C. O. Justice, E. F. Moran, J. F. Mustard, R. R. Rindfuss, D. Skole, B. L. Turner II, and M. A. Cochrane. 2004. *Land Change Science: Observing, Monitoring and Understanding Trajectories of Change on the Earth's Surface* (Vol. 6). Dordrecht: Kluwer Academic Publishers.
- Hu, X., and Q. Weng. 2009. "Estimating Impervious Surfaces from Medium Spatial Resolution Imagery Using the Self-Organizing Map and Multi-Layer Perceptron Neural Networks." *Remote Sensing of Environment* 113 (10): 2089–2102. doi:10.1016/j.rse.2009.05.014.
- Huang, C., L. S. Davis, and J. R. G. Townshend. 2002. "An Assessment of Support Vector Machines for Land Cover Classification." *International Journal of Remote Sensing* 23 (4): 725–749. doi:10.1080/01431160110040323.
- Huang, C., B. Wylie, L. Yang, C. Homer, and G. Zylstra. 2002. "Derivation of a Tasseled Cap Transformation Based on Landsat 7 At-Satellite Reflectance." *International Journal of Remote Sensing* 23 (8): 1741–1748. doi:10.1080/01431160110106113.
- Huang, D., and C. Wang. 2009. "Optimal Multi-Level Thresholding Using a Two-Stage Otsu Optimization Approach." *Pattern Recognition Letters* 30 (3): 275–284. doi:10.1016/j.patrec.2008.10.003.
- Li, G., D. Lu, E. Moran, and S. Hetrick. 2013. "Mapping Impervious Surface Area in the Brazilian Amazon Using Landsat Imagery." *Giscience & Remote Sensing* 50: 172–183. doi:10.1080/15481603.2013.780452.
- Li, X., P. Gong, and L. Liang. 2015. "A 30-Year (1984–2013) Record of Annual Urban Dynamics of Beijing City Derived from Landsat Data." *Remote Sensing of Environment* 166: 78–90. doi:10.1016/j.rse.2015.06.007.
- Ma, Y., and R. Xu. 2010. "Remote Sensing Monitoring and Driving Force Analysis of Urban Expansion in Guangzhou City, China." *Habitat International* 34 (2): 228–235. doi:10.1016/j.habitatint.2009.09.007.
- Mitraka, Z., N. Chrysoulakis, Y. Kamarianakis, P. Partsinevelos, and A. Tsouchlaraki. 2012. "Improving the Estimation of Urban Surface Emissivity Based on Sub-Pixel Classification of High Resolution Satellite Imagery." *Remote Sensing of Environment* 117: 125–134. doi:10.1016/j.rse.2011.06.025.

- Otsu, N. 1979. "A Threshold Selection Method from Gray-Level Histograms." *IEEE Transactions on Systems, Man, and Cybernetics* 9 (1): 62–66. doi:10.1109/TSMC.1979.4310076.
- Poursanidis, D., N. Chrysoulakis, and Z. Mitraka. 2015. "Landsat 8 Vs. Landsat 5: A Comparison Based on Urban and Peri-Urban Land Cover Mapping." *International Journal of Applied Earth Observation and Geoinformation* 35: 259–269. doi:10.1016/j.jag.2014.09.010.
- Ridd, M. 1995. "Exploring a V–I–S (Vegetation–Impervious–Surface–Soil) Model for Urban Ecosystem Analysis through Remote Sensing: Comparative Anatomy for Cities." *International Journal of Remote Sensing* 16: 2165–2185. doi:10.1080/01431169508954549.
- Rikimaru, A. 1996. "Landsat TM Data Processing Guide for Forest Canopy Density Mapping and Monitoring Model." In *International Tropical Timber Organization (ITTO) Workshop on Utilization of Remote Sensing in Site Assessment and Planning for Rehabilitation of Logged-Over Forest, Bangkok, Thailand, July-August 1*.
- Rosenfield, G. H., and K. Fitzpatrick-Lins. 1986. "A Coefficient of Agreement as A Measure of Thematic Classification Accuracy." *Photogrammetric Engineering and Remote Sensing* 52 (2): 223–227.
- Rouse, J., R. Haas, J. Schell, and D. Deering. *Monitoring Vegetation Systems in the Great Plains with ERTS*. Third ERTS Symposium, NASA (1973): 309–317.
- Schneider, A., and C. M. Mertes. 2014. "Expansion and Growth in Chinese Cities, 1978–2010." *Environmental Research Letters* 9 (2): 1748–9326. doi:10.1088/1748-9326/9/2/024008.
- Schneider, A., K. C. Seto, and D. R. Webster. 2005. "Urban Growth in Chengdu, Western China: Application of Remote Sensing to Assess Planning and Policy Outcomes." *Environment and Planning B: Planning and Design* 32 (3): 323–345. doi:10.1068/b31142.
- Seto, K. C., C. E. Woodcock, C. Song, X. Huang, J. Lu, and R. K. Kaufmann. 2002. "Monitoring Land-Use Change in the Pearl River Delta Using Landsat TM." *International Journal of Remote Sensing* 23 (10): 1985–2004. doi:10.1080/01431160110075532.
- Shao, M., X. Tang, Y. Zhang, and W. Li. 2006. "City Clusters in China: Air and Surface Water Pollution." *Frontiers in Ecology and the Environment* 4 (7): 353–361. doi:10.1890/1540-9295(2006)004[0353:CCICAA]2.0.CO;2.
- Somers, B., M. Zortea, A. Plaza, and G. P. Asner. 2012. "Automated Extraction of Image-Based Endmember Bundles for Improved Spectral Unmixing." *IEEE Journal of Selected Topics in Applied Earth Observations and Remote Sensing* 5 (2): 396–408. doi:10.1109/JSTARS.2011.2181340.
- Story, M., and R. G. Congalton. 1986. "Accuracy Assessment - A User's Perspective." *Photogrammetric Engineering and Remote Sensing* 52 (3): 397–399.
- Sun, C., Z. F. Wu, Z. Q. Lv, N. Yao, and J. B. Wei. 2013. "Quantifying Different Types of Urban Growth and the Change Dynamic in Guangzhou Using Multi-Temporal Remote Sensing Data." *International Journal of Applied Earth Observation and Geoinformation* 21: 409–417. doi:10.1016/j.jag.2011.12.012.
- Swain, P. H., and S. M. Davis. 1978. *Remote Sensing: the Quantitative Approach*. New York: McGraw-Hill.
- Triantakoustantis, D., N. Chrysoulakis, A. Sazonova, T. Esch, C. Feigenwinter, S. Düzgün, E. Parlow, M. Marconcini, and A. Tal. 2015. "On-Line Evaluation of Earth Observation Derived Indicators for Urban Planning and Management." *Urban Plan and Design Research* 3: 17–33. doi:10.14355/updr.2015.03.003.
- Vapnik, V. 1995. *The Nature of Statistical Learning Theory*. New York: Springer-Verlag.
- Vapnik, V. 1998. *Statistical Learning Theory*, 1. Wiley: New York.
- Vieira, M. A., A. R. Formaggio, C. D. Rennó, C. Atzberger, D. A. Aguiar, and M. P. Mello. 2012. "Object Based Image Analysis and Data Mining Applied to a Remotely Sensed Landsat Time-Series to Map Sugarcane over Large Areas." *Remote Sensing of Environment* 123: 553–562. doi:10.1016/j.rse.2012.04.011.
- Weng, Q. 2001. "A Remote Sensing and GIS Evaluation of Urban Expansion and Its Impact on Surface Temperature in the Zhujiang Delta, China." *International Journal of Remote Sensing* 22 (10): 1999–2014. doi:10.1080/713860788.
- Weng, Q. 2012. "Remote Sensing of Impervious Surfaces in the Urban Areas: Requirements, Methods, and Trends." *Remote Sensing of Environment* 117: 34–49. doi:10.1016/j.rse.2011.02.030.

- Woodcock, C. E., R. Allen, M. Anderson, A. Belward, R. Bindschadler, W. Cohen, F. Gao, et al. 2008. "Free Access to Landsat Imagery." *Science (New York, NY)* 320 (5879): 1011. doi:10.1126/science.320.5879.1011a.
- Xu, H. 2005. "A Study on Information Extraction of Water Body with the Modified Normalized Difference Water Index (MNDWI)." *Journal of Remote Sensing* 5: 589–595.
- Xu, H. 2010. "Analysis of Impervious Surface and Its Impact on Urban Heat Environment Using the Normalized Difference Impervious Surface Index (NDISI)." *Photogrammetric Engineering & Remote Sensing* 76 (5): 557–565. <http://dx.doi.org/10.14358/PERS.76.5.557>.
- Zha, Y., J. Gao, and S. Ni. 2003. "Use of Normalized Difference Built-Up Index in Automatically Mapping Urban Areas from TM Imagery." *International Journal of Remote Sensing* 24 (3): 583–594. doi:10.1080/01431160304987.
- Zhang, C., Y. Chen, and D. Lu. 2015. "Mapping the Land-Cover Distribution in Arid and Semiarid Urban Landscapes with Landsat Thematic Mapper Imagery." *International Journal of Remote Sensing* 36 (17): 4483–4500. doi:10.1080/01431161.2015.1084552.
- Zhang, X., T. Kang, H. Wang, and Y. Sun. 2010. "Analysis on Spatial Structure of Landuse Change Based on Remote Sensing and Geographical Information System." *International Journal of Applied Earth Observation and Geoinformation* 12: S145–S150. doi:10.1016/j.jag.2010.04.011.
- Zhou, L., R. E. Dickinson, Y. Tian, J. Fang, Q. Li, R. K. Kaufmann, C. J. Tucker, and R. B. Myneni. 2004. "Evidence for a Significant Urbanization Effect on Climate in China." *Proceedings of the National Academy of Sciences of the United States of America* 101 (26): 9540–9544. doi:10.1073/pnas.0400357101.